Eur. Phys. J. C (2010) 65: 637–647
DOI 10.1140/epjc/s10052-009-1202-0

THE EUROPEAN PHYSICAL JOURNAL C

Special Article - Tools for Experiment and Theory

LHC as πp and $\pi\pi$ collider

V.A. Petrov[a], **R.A. Ryutin**[b], **A.E. Sobol**[c]

Institute for High Energy Physics, 142 281 Protvino, Russia

Received: 20 July 2009 / Revised: 13 October 2009 / Published online: 1 December 2009

Abstract We propose an experiment at the LHC with leading neutron production. The latter can be used to extract from it the total $\pi^+ p$ cross-sections. With two leading neutrons we can get access to the total $\pi^+\pi^+$ cross-sections. In this note we give some estimates and discuss related problems and prospects.

PACS 11.55.Jy · 12.40.Nn · 13.85.Lg · 13.85.Ni

1 Introduction

The Large Hadron Collider, LHC, opens up new possibilities for diffractive physics, especially in measurements of the total and elastic pp cross-sections. These will allow us to discriminate among many models of high-energy diffractive scattering. However, the pp cross-sections results will not be sufficient to separate all viable models. For this we need the information on the high-energy cross-sections of other initial states. On quite general grounds we expect a universal high-energy behavior of any total cross-section, independently of the initial state. Unfortunately, apart from pp and $\bar{p}p$ collisions we have only rather low energy data. For instance, the total cross-section of $\pi^+ p$ interaction is known only up to 25 GeV. At present no plans exist to get high-energy secondary beams to fill this gap. Nonetheless, we can use an old idea of Goebel and Chew-Low [1, 2] based on virtual particles and poles in the scattering matrix to extract such cross sections. For example, in Refs. [3–5] total and elastic $\pi\pi$ cross-sections were extracted in the energy domain 1.5–4.0 GeV from the cross-sections of exclusive processes with charge exchange. In Ref. [6] $\pi^-\pi^-$ cross-sections were extracted from the reaction $\pi^- + n \to p + X$ for energies up to 18.4 GeV. More recently the πp cross section at $\sqrt{s} = 50$ GeV was extracted from the $\gamma + p \to \pi^+ + \pi^- + p$ process [7] with a (model dependent [8, 9]) result of $\sigma_{\pi p}(50\,\text{GeV}) = 31 \pm 2\,(\text{stat.}) \pm 3\,(\text{syst.})$ mb. At LHC it will be difficult to measure exclusive channels. As an alternative we propose to measure the inclusive spectra of fast leading neutrons in order to deduce pion cross-sections in the energy range 1–5 TeV.

The process of leading neutron production has been studied at several experiments in photon-hadron [10–17] and hadron-hadron [18–24] colliders. In this paper we consider processes of the type $p + p \to n + X$ and $p + p \to n + X + n$. As was noted in [25], the experimental study of charge exchange in hadron-hadron collisions is not so clear. Some experiments are in agreement with the theoretical expectations [23, 24], while others [18] are not. Since leading neutron production is dominated by π exchange [25–28] we have a chance to extract total $\pi^+ p$ and $\pi^+\pi^+$ cross-sections in a relatively model independent way. This is the motivation for this paper.

At high energies we have to take into account effects of soft rescattering which can be calculated as corrections to the Born approximation. In the calculations of such absorptive effects we use Regge-eikonal approach [29]. In the first part of the paper we present our calculations for differential cross-sections, while in the last section the Monte-Carlo simulation and experimental possibilities are considered using the CMS ZDC [30, 31] detector as an example.

2 Kinematics

The diagram of the Single pion Exchange (SπE) process $p + p \to n + X$ is presented in Fig. 1a. The momenta are p_1, p_2, p_n, p_X respectively. In the center-of-mass frame these can be represented as follows (boldface letters denote transverse momenta):

$$p_1 = \left(\frac{\sqrt{s}}{2}, \frac{\sqrt{s}}{2}\beta, \mathbf{0}\right), \qquad p_2 = \left(\frac{\sqrt{s}}{2}, -\frac{\sqrt{s}}{2}\beta, \mathbf{0}\right). \tag{1}$$

[a] e-mail: vladimir.petrov@cern.ch
[b] e-mail: roman.rioutine@cern.ch
[c] e-mail: andrei.sobol@cern.ch

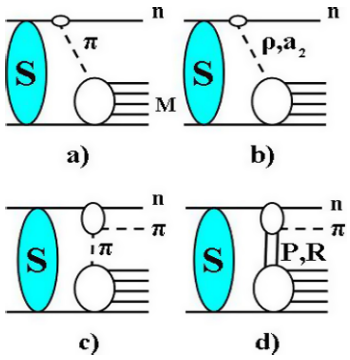

Fig. 1 Diagrams for the signal and background processes in pp collisions. **a** process with a single pion exchange $p+p\to n+X$, M is the mass of the system X; **b** process with other reggeon exchanges; **c** double dissociation process with a pion exchange; **d** double dissociation with Pomeron and reggeon exchanges. S represents soft rescattering corrections

With this notation, the momentum of the π is

$$p_\pi = \left(\xi\frac{\sqrt{s}}{2}\beta^2 + \frac{t+m_p^2-m_n^2}{\sqrt{s}}, \xi\frac{\sqrt{s}}{2}\beta, \mathbf{q}\right), \tag{2}$$

and

$$p_n = p_1 - p_\pi, \tag{3}$$

$$p_X^2 = M^2, \tag{4}$$

$$\xi = \frac{M^2 - m_n^2 - 2(t+m_p^2-m_n^2)}{s\beta^2} \simeq \frac{M^2}{s}, \tag{5}$$

$$-t = \frac{\mathbf{q}^2 + \xi^2\beta^2 m_p^2 + (m_n^2-m_p^2)(\xi\beta^2 - \frac{m_n^2-m_p^2}{s})}{1-\xi\beta^2+\frac{2(m_n^2-m_p^2)}{s}}$$

$$\simeq \frac{\mathbf{q}^2+\xi^2 m_p^2}{1-\xi}, \tag{6}$$

$$\beta = \sqrt{1-\frac{4m_p^2}{s}}. \tag{7}$$

One of the important questions is the definition of the kinematical region of the process, especially in rapidity y (pseudorapidity η) (see Section 5). If we have several secondaries from $\pi^+ p$ scattering with momenta

$$k_i = \left(\sqrt{m_i^2+\mathbf{k}_i^2+\xi_i^2\beta^2\frac{s}{4}}, -\xi_i\beta\frac{\sqrt{s}}{2}, \mathbf{k}_i\right) \tag{8}$$

then

$$\sum_i \xi_i = 1-\xi, \qquad \sum_i \mathbf{k}_i = \mathbf{q},$$

$$\sum_i \sqrt{\xi_i^2 + \frac{4(m_i^2+\mathbf{k}_i^2)}{s\beta^2}}$$

$$= 1+\xi\beta^2 + \frac{t+m_p^2-m_n^2}{\sqrt{s}} \simeq 1+\xi, \tag{9}$$

and

$$y_i \simeq \frac{1}{2}\ln\frac{(\sqrt{\xi_i^2+\frac{4(m_i^2+\mathbf{k}_i^2)}{s}}-\xi_i)^2}{\frac{4(m_i^2+\mathbf{k}_i^2)}{s}}, \tag{10}$$

$$\eta_i \simeq \frac{1}{2}\ln\frac{(\sqrt{\xi_i^2+\frac{4\mathbf{k}_i^2}{s}}-\xi_i)^2}{\frac{4\mathbf{k}_i^2}{s}}. \tag{11}$$

For negative ξ_i we have $y_i \to y_{i,\max}$, $\eta_i\to\infty$ for $\mathbf{k}_i\to 0$. This means that when we produce soft hadrons we have no pseudorapidity gap even in the case when the rapidity is

$$y_{i,\max} \simeq \ln\frac{\xi_i\sqrt{s}}{m_i} \le \ln\frac{M^2}{\sqrt{s}m_i}. \tag{12}$$

Experimentally this puts us in the difficult situation of having to cut soft particles in order to see the pseudorapidity gap. For example, if $y=6$ for pions of energy 30 GeV, then $\eta\simeq 9$ is close to the beam.

3 Calculation of the cross-section. Absorptive effects

As a Born approximation for π exchange we use the familiar triple-Regge formula (see Fig. 2). This formula can be rewritten as

$$\frac{d\sigma_0(p+p\to n+X)}{d\xi dt} = \frac{G^2_{\pi^+pn}}{16\pi^2}\frac{-t}{(t-m_\pi^2)^2}F^2(t)\xi^{1-2\alpha_\pi(t)}\sigma_{\pi^+p}(\xi s), \tag{13}$$

where the pion trajectory is $\alpha_\pi(t)=\alpha'_\pi(t-m_\pi^2)$. The slope $\alpha'\simeq 0.9$ GeV^{-2}, $\xi=1-x_L$, were x_L is the fraction of the initial proton's longitudinal momentum carried by the neutron, and $G^2_{\pi^0pp}/(4\pi)=G^2_{\pi^+pn}/(8\pi)=13.75$ [32, 33]. The form factor $F(t)$ is usually expressed as an exponential

$$F(t)=\exp(bt), \tag{14}$$

where, from recent data [14, 34], we expect $b\simeq 0.3$ GeV^{-2}. We are interested in the kinematical range

$$\xi<0.4, \qquad 0.01<|t|<0.5\ \text{GeV}^2,$$

where formula (13) dominates according to [35] and [36]. At high energies we can use any adequate parametrization of the total π^+p cross-sections.

Apart from pion exchange, Fig. 1a other processes such as ρ and a_2 exchange (Fig. 1b), resonance (Δ, N^*) decays

(Fig. 1c, d) can produce leading neutrons [34–36]. Pion exchange dominates while ρ and a_2 exchange contribution is about 20%. The other reggeons only give small contributions due to spin effects [34]. The main background comes from minimum bias events and the pomeron exchange double dissociation process, see Fig. 1d. This was estimated to be about $0.06 \cdot \sigma(p+p \to p+X)$ [37] at low energies. It has, however, an inverse missing mass dependence and is suppressed at intermediate ξ (see Fig. 3). This fact is used to eliminate the background.

Another important suppression factor arises from absorptive corrections [25]. We estimate only absorption in the initial state, since it gives the main contribution. For this task we use our model with 3 Pomeron trajectories [29]:

$$\begin{aligned}
&\alpha_{IP_1}(t) - 1 = (0.0578 \pm 0.002) + (0.5596 \pm 0.0078)t,\\
&\alpha_{IP_2}(t) - 1 = (0.1669 \pm 0.0012) + (0.2733 \pm 0.0056)t,\\
&\alpha_{IP_3}(t) - 1 = (0.2032 \pm 0.0041) + (0.0937 \pm 0.0029)t.
\end{aligned} \tag{15}$$

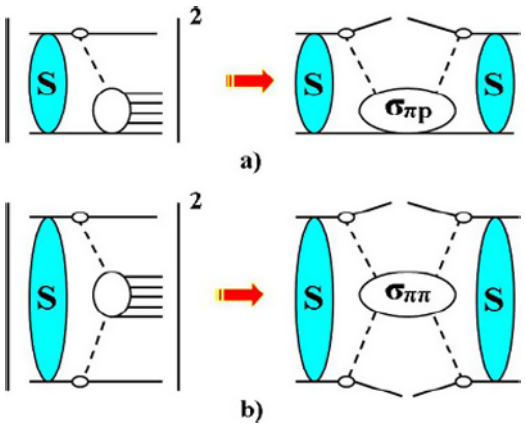

Fig. 2 Amplitudes squared and total cross-sections of the processes: **a** $p+p \to n+X$ (SπE), **b** $p+p \to n+X+n$ (DπE). S represents soft rescattering corrections

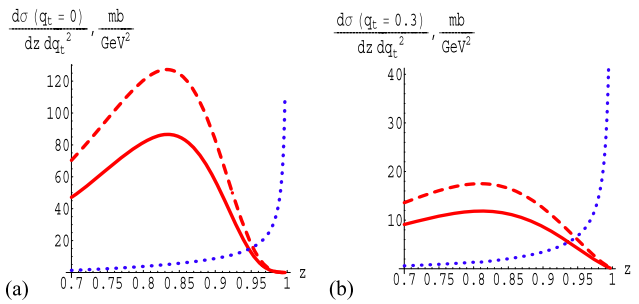

Fig. 3 Differential cross-sections for the processes $p+p \to n+X$ (parametrization (31), *solid*, and (32), *dashed*) and double dissociation process $p+p \to N^*(\to n+\pi)+X$ (*dotted*) at different values of transverse momentum transfer versus $z = 1-\xi$

These trajectories are the result of a 20 parameter fit of the total and differential cross-sections in the region

$$0.01 < |t| < 14\ \text{GeV}^2,$$

$$8 < \sqrt{s} < 1800\ \text{GeV}.$$

Although the $\chi^2/\text{d.o.f.} = 2.74$ is rather large, the model gives good predictions for the elastic scattering (especially in the low-t region with $\chi^2/\text{d.o.f.} \sim 1$).

We use the procedure described in [27, 28] to estimate the absorptive corrections. With an effective factorized form of the, here-under, expression (17) used for convenience, we obtain:

$$\begin{aligned}
&\frac{d\sigma_0(\xi,\mathbf{q}^2)}{d\xi d\mathbf{q}^2}\\
&\quad = \left(m_p^2\xi^2 + \mathbf{q}^2\right)\left|\Phi_B\left(\xi,\mathbf{q}^2\right)\right|^2 \frac{\xi}{(1-\xi)^2}\sigma_{\pi^+p}(\xi\, s),
\end{aligned} \tag{16}$$

$$\frac{d\sigma(s/s_0,\xi,\mathbf{q}^2)}{d\xi d\mathbf{q}^2} = S\left(s/s_0,\xi,\mathbf{q}^2\right)\frac{d\sigma_0(\xi,\mathbf{q}^2)}{d\xi d\mathbf{q}^2}, \tag{17}$$

$$S = \frac{m_p^2\xi^2|\Phi_0(s/s_0,\xi,\mathbf{q}^2)|^2 + \mathbf{q}^2|\Phi_s(s/s_0,\xi,\mathbf{q}^2)|^2}{(m_p^2\xi^2+\mathbf{q}^2)|\Phi_B(\xi,\mathbf{q}^2)|^2}. \tag{18}$$

The functions Φ_0 and Φ_s arise from different spin contributions to the amplitude

$$A_{p\to n} = \frac{1}{\sqrt{1-\xi}}\bar{\Psi}_n\left(m_p\xi\hat{\sigma}_3\cdot\Phi_0 + \mathbf{q}\hat{\boldsymbol{\sigma}}\cdot\Phi_s\right)\Psi_p \tag{19}$$

and both are equal to Φ_B in the Born approximation. Here $\hat{\sigma}_i$ are Pauli matrices and $\bar{\Psi}_n$, Ψ_p are neutron and proton spinors. All the above functions can be calculated from the following formulae:

$$\begin{aligned}
\Phi_B\left(\xi,\mathbf{q}^2\right) &= \frac{N(\xi)}{2\pi}\left(\frac{1}{\mathbf{q}^2+\epsilon^2} + \imath\frac{\pi\alpha'_\pi}{2(1-\xi)}\right)\exp\left(-\beta^2\mathbf{q}^2\right)\\
&\simeq \frac{N(\xi)}{2\pi}\frac{1}{\mathbf{q}^2+\epsilon^2}\frac{1}{1+\beta^2\mathbf{q}^2}, \quad \mathbf{q}\to 0,
\end{aligned} \tag{20}$$

$$N(\xi) = (1-\xi)\frac{G_{\pi^+pn}}{2}\xi^{\frac{\alpha'_\pi\epsilon^2}{1-\xi}}\exp\left[-b\frac{m_p^2\xi^2}{1-\xi}\right], \tag{21}$$

$$\beta^2 = \frac{b+\alpha'_\pi\ln\frac{1}{\xi}}{1-\xi}, \qquad \epsilon^2 = m_p^2\xi^2 + m_\pi^2(1-\xi), \tag{22}$$

$$\Theta_0\left(b,\xi,|\mathbf{q}|\right) = \frac{bJ_0(b|\mathbf{q}|)(K_0(\epsilon b) - K_0(\frac{b}{\beta}))}{1-\beta^2\epsilon^2}, \tag{23}$$

$$\Theta_s\left(b,\xi,|\mathbf{q}|\right) = \frac{bJ_1(b|\mathbf{q}|)(\epsilon K_1(\epsilon b) - \frac{1}{\beta}K_1(\frac{b}{\beta}))}{1-\beta^2\epsilon^2}, \tag{24}$$

$$\Phi_0 = \frac{N(\xi)}{2\pi}\int_0^\infty db\,\Theta_0\left(b,\xi,|\mathbf{q}|\right)V(b), \tag{25}$$

$$|\mathbf{q}|\Phi_s = \frac{N(\xi)}{2\pi}\int_0^\infty db\,\Theta_s\big(b,\xi,|\mathbf{q}|\big)V(b), \tag{26}$$

$$V(b) = \exp\big(-\Omega_{\rm el}(s/s_0,b)\big), \tag{27}$$

$$\Omega_{\rm el} = \sum_{i=1}^{3}\Omega_i, \tag{28}$$

$$\Omega_i = \frac{2c_i}{16\pi B_i}\left(\frac{s}{s_0}\mathrm{e}^{-\imath\frac{\pi}{2}}\right)^{\alpha_{IP_i}(0)-1}\exp\left[-\frac{b^2}{4B_i}\right], \tag{29}$$

$$B_i = \alpha'_{IP_i}\ln\left(\frac{s}{s_0}\mathrm{e}^{-\imath\frac{\pi}{2}}\right) + \frac{r_i^2}{4}. \tag{30}$$

The values of the parameters c_i and r_i^2 are derived in (15) and listed in Table 1.

For π^+p interaction we use, for example, the Donnachie–Landshoff cross-section [38]

$$\sigma_{\pi^+p}(s) = 13.63s^{0.0808} + 25.56s^{-0.4525}\ \text{(mb)} \tag{31}$$

and also the COMPETE one [39]

$$\sigma_{\pi^+p}(s) = Z_{\pi p} + B\ln^2\left(\frac{s}{s_0}\right) + \big(Y_+s^{\alpha_+} - Y_-s^{\alpha_-}\big)/s\ \text{(mb)}, \tag{32}$$

$$Z_{\pi p} = 21.23 \pm 0.33\ \text{mb},$$
$$B = 0.3152 \pm 0.0095\ \text{mb}, \tag{33}$$

$$s_0 = 34 \pm 5.4\ \text{GeV}^2, \tag{34}$$

$$Y_+ = 17.8 \pm 1.1, \qquad \alpha_+ = 0.533 \pm 0.015, \tag{35}$$

$$Y_- = 5.72 \pm 0.16, \qquad \alpha_- = 0.4602 \pm 0.0064 \tag{36}$$

to make predictions for ISR [18] and PHENIX [24]. The results are depicted in Fig. 4 for parametrizations (31) and (32). It is clear from the figures, that the calculated cross-section is about 1.7 factor lower than experimental points, this discrepancy is discussed in [27]: it may reflect a wrong normalization of the ISR data, since the new data [23, 24] are lower and closer to predictions of the model as depicted in Fig. 5.

We can of course use any other reliable parametrization. Nevertheless our principal aim is *to extract* $\sigma_{\pi^+p}(s)$ *from the data*. One method [1] is to evaluate the factor in front of σ_{π^+p} in (13) at some low $t \simeq -0.014$, and then divide the data by this factor. For a fixed value of t we obtain $\xi \simeq 0.125$ for $\mathbf{q} \sim 0$. From measurements at the ISR [18] we can read off the cross-section $E\,d\sigma/d^3p$ at $x = 1-\xi = 0.875$. This yields an approximate formula for the total π^+p cross-section

$$\begin{aligned}\sigma_{\pi^+p}&(0.125\ \text{s})\\ &\simeq \frac{\pi}{1.7(3\ \text{GeV}^{-2})S(s/s_0,0.125,0)}\left(E\frac{d\sigma(\mathbf{q}\sim 0)}{d^3p}\right)\\ &\simeq (0.9\ \text{GeV}^2)\left(E\frac{d\sigma(\mathbf{q}\sim 0)}{d^3p}\right),\end{aligned} \tag{37}$$

where $S(s/s_0,0.125,0) \simeq 0.68$. For low energies this formula gives reasonable predictions for the cross-section (see Table 2 and Fig. 6) which are compatible with real π^+p

Table 1 Parameters of the model

i	1	2	3
c_i	53.0 ± 0.8	9.68 ± 0.16	1.67 ± 0.07
r_i^2 (GeV^{-2})	6.3096 ± 0.2522	3.1097 ± 0.1817	2.4771 ± 0.0964

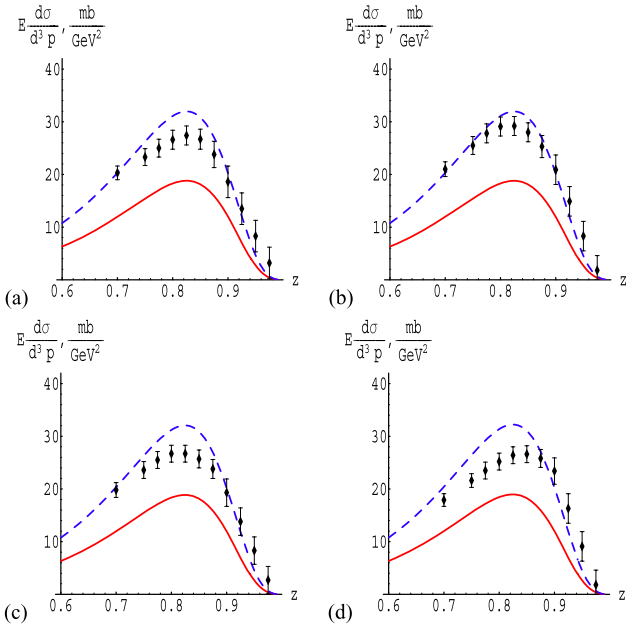

Fig. 4 Theoretical differential cross-section $E\,d\sigma/d^3p$ in mb/GeV^2 versus ISR data [18] for $|\mathbf{q}| \sim 0$: **a** $\sqrt{s} = 30.6$ GeV, **b** $\sqrt{s} = 44.9$ GeV, **c** $\sqrt{s} = 52.8$ GeV, **d** $\sqrt{s} = 62.7$ GeV. *Lower curves* are the theoretical predictions and upper curve are the predictions multiplied by factor 1.7

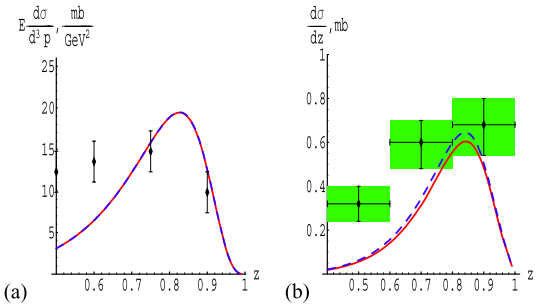

Fig. 5 Theoretical differential cross-sections: **a** $E\,d\sigma/d^3p$ in mb/GeV^2 versus NA49 data [23] at $\sqrt{s} = 17.2$ GeV for $|\mathbf{q}| \sim 0$; **b** $d\sigma/dz$ in mb versus PHENIX data [24] at $\sqrt{s} = 200$ GeV, from parametrizations (31) (*solid*) and (32) (*dashed*). Two curves coincide in (**a**)

measurements [40] if we take into account reggeon corrections.

An exact extraction procedure is more delicate since we have to extrapolate doubly differential SπE cross-sections to the value $t = m_\pi^2 > 0$ and then apply the procedure described in the previous paragraph. Experimentally this is rather difficult (see Sect. 5), since errors in t are larger than m_π^2. To get around this problem we extract cross-sections for pions with low virtualities and assume that these values are close to reality. Figure 7 shows S, the model dependent survival fraction described by (18). At $t \to 0$ it tends to unity and so we can obtain a more model independent cross-section $\sigma_{\pi^+ p}$.

The differential cross-sections for the process $p + p \to n + X$ at $\sqrt{s} = 10$ TeV are depicted in Figs. 8 and 9 for both the Donnachie–Landshoff (31) and COMPETE (32) parametrizations. The total cross sections are listed in Table 3. They are in the range 40–1300 μb for all values of $\xi_{\max}$ implying that we will have plenty of rate for the measurements.

Total absorptive corrections $\sigma_{0,S\pi E}/\sigma_{S\pi E}$ are about 0.35 in the kinematical region $10^{-6} < \xi < \xi_{\max} = 0.15$, $0.01\ \text{GeV}^2 < |t| < 0.5\ \text{GeV}^2$. The ratio of corrected to Born cross-sections is rather small even for low t and ξ values (see Fig. 8). This fact is not surprising because the integration of the doubly differential SπE cross-section in t or ξ includes regions where absorption is strong.

Table 2 Total $\pi^+ p$ cross-sections extracted from the ISR [18], NA49 [23] (first numbers), HERA [7] and PHENIX [24] (last two numbers) data. The last row shows numbers from COMPETE parametrization (32)

$\sqrt{s}$, GeV	$\sigma_{\pi^+ p}$, mb	$\sigma^{\text{exp.}}_{\pi^+ p}$, mb
9.4	20 ± 3.75	23.2
10.8	21.4 ± 2.3	23.19
15.9	22.8 ± 1.9	23.55
18.7	21.4 ± 1.6	23.85
22.2	23.2 ± 1.5	24.27
50	31 ± 3.6	27.43
70	25.9 ± 4.5	29.3

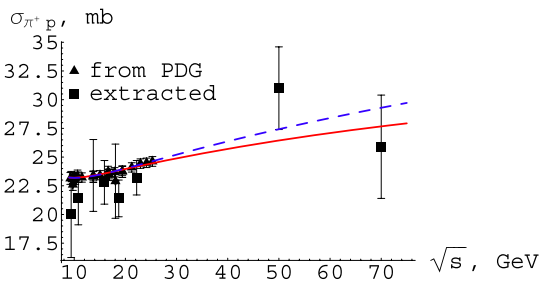

Fig. 6 $\sigma_{\pi^+ p}$ extracted from data [7, 18, 23, 24] and measured in real experiments [40]. Two parametrizations (31) (*solid*) and (32) (*dashed*) are also shown

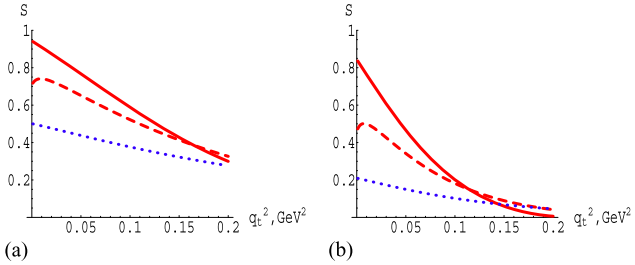

Fig. 7 Function $S(s/s_0, \xi, q_t)$ at **a** $\sqrt{s} = 62.7$ GeV and **b** $\sqrt{s} = 10$ TeV for different ξ values: $\xi = 0.3$ (*dotted*), $\xi = 0.1$ (*dashed*) and $\xi = 10^{-4}$ (*solid*)

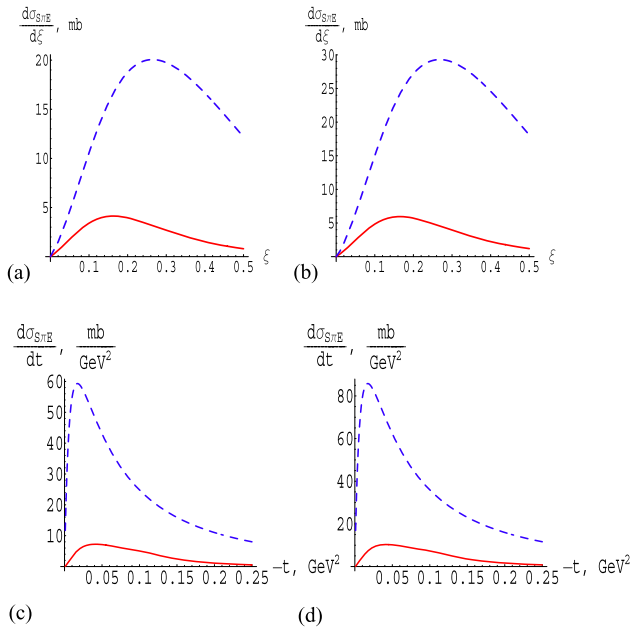

Fig. 8 Partly integrated SπE cross-sections at $\sqrt{s} = 10$ TeV: **a**, **b** $d\sigma/d\xi$, $0.01\ \text{GeV}^2 < |t| < 0.5\ \text{GeV}^2$; **c**, **d** $d\sigma/dt$, $10^{-4} < \xi < 0.3$ for Donnachie–Landshoff (31) (**a**, **c**) and COMPETE (32) (**b**, **d**) parametrizations. Born cross-sections (integrated (16)) are depicted as *dashed curves* and corrected (integrated (17)) cross-sections are shown by *solid curves*

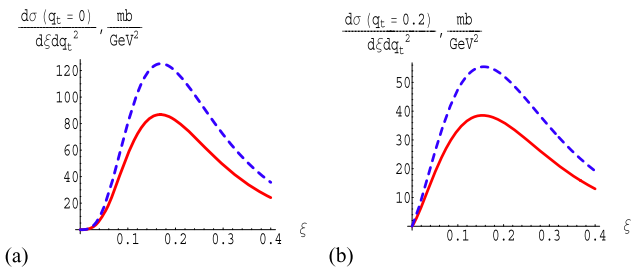

Fig. 9 Doubly differential SπE cross-sections $d\sigma/d\xi\, d\mathbf{q}^2$ at $\sqrt{s} = 10$ TeV for Donnachie–Landshoff (31) (*solid*) and COMPETE (32) (*dashed*) parametrizations at two different values of $|\mathbf{q}|$: **a** $|\mathbf{q}| = 0$ GeV and **b** $|\mathbf{q}| = 0.2$ GeV

Table 3 Total $p+p\to n+X$ cross-sections in the kinematical region $0<|\mathbf{q}|<0.5$ GeV, $\xi_{\min}=10^{-6}<\xi<\xi_{\max}$ for two parametrizations (31) (32)

$\xi_{\max}$	0.05	0.1	0.2	0.3
$\sigma_{p+p\to n+X}$, μb	42(57)	175(244)	576(820)	921(1320)

At low energies the region of applicability of our model is given by the inequalities

$$0.01\ \text{GeV}^2<|t|<0.5\ \text{GeV}^2,\qquad 10^{-6}<\xi<0.4. \tag{38}$$

At higher energies this region may be smaller (say $\xi<0.1$), since this corresponds to masses $M=3$ TeV at $\sqrt{s}=10$ TeV, and for large masses the formalism may break down.

4 Double pion exchange

As noted above, the Double pion Exchange (DπE) inclusive process can give information on both total and elastic $\pi\pi$ cross-sections. $\pi\pi$ cross-sections have been extracted in the past using exclusive cross-section [5]. These attempts are shown in Fig. 10. There is some tendency of the early flattening of the $\pi\pi$ cross-sections. In πp and pp cross-sections this flattening begins at higher energies and precedes further growth. Figure 11 shows the cross sections for $\pi\pi$ interactions [6]. It is not clear if there is an early beginning in the growth of the cross section or not.

We can extend the analysis for one pion exchange described above to double pion exchange (Fig. 2b, DπE). The kinematics is similar to the double pomeron exchange process:

$$p_{\pi_i}\simeq\left(\xi_i\frac{\sqrt{s}}{2},(-1)^{i-1}\xi_i\frac{\sqrt{s}}{2},\mathbf{q}_i\right), \tag{39}$$

$$p_{ni}=p_i-p_{\pi_i}, \tag{40}$$

$$\begin{aligned}p_X^2=M^2&=\xi_1\xi_2 s\beta^2\frac{1+\beta^2}{2}t(\mathbf{q}_1+\mathbf{q}_2)^2\\&\quad-m_p^2\beta^2\big(\xi_1^2+\xi_2^2\big)+\big(t_1+t_2+2\big(m_p^2-m_n^2\big)\big)\\&\quad\times\left(\beta^2(\xi_1+\xi_2)+\frac{t_1+t_2+2(m_p^2-m_n^2)}{s}\right)\\&\simeq\xi_1\xi_2 s,\end{aligned} \tag{41}$$

$$-t_i\simeq\frac{\mathbf{q}_i^2+\xi_i^2m_p^2}{1-\xi_i}. \tag{42}$$

The cross-section can be evaluated as follows:

$$\begin{aligned}&\frac{d\sigma_0(\xi_1,\xi_2,\mathbf{q}_1^2,\mathbf{q}_2^2)}{d\xi_1\,d\xi_2\,d\mathbf{q}_1^2\,d\mathbf{q}_2^2}\\&\quad=\prod_{i=1}^{2}\left[\big(m_p^2\xi_i^2+\mathbf{q}_i^2\big)\big|\Phi_B\big(\xi_i,\mathbf{q}_i^2\big)\big|^2\frac{\xi_i}{(1-\xi_i)^2}\right]\\&\qquad\times\sigma_{\pi^+\pi^+}(\xi_1\xi_2 s),\end{aligned} \tag{43}$$

$$d\sigma=S_2\big(s/s_0,\xi_{1,2},\mathbf{q}_{1,2}^2\big)\,d\sigma_0, \tag{44}$$

$$S_2=\frac{\sum_{i,j=0,s}\rho_{ij}^2|\bar{\Phi}_{ij}(s/s_0,\xi_{1,2},\mathbf{q}_{1,2}^2)|^2}{\prod_{i=1}^2[(m_p^2\xi_i^2+\mathbf{q}_i^2)|\Phi_B(\xi_i,\mathbf{q}_i^2)|^2]}, \tag{45}$$

$$\begin{aligned}\bar{\Phi}_{ij}&=\frac{N(\xi_1)N(\xi_2)}{(2\pi)^2}\\&\quad\times\int_0^\infty db_1\,db_2\,\Theta_i\big(b_1,\xi_1,|\mathbf{q}_1|\big)\Theta_j\big(b_2,\xi_2,|\mathbf{q}_2|\big)\\&\quad\times I_\phi(b_1,b_2),\end{aligned} \tag{46}$$

$$I_\phi(b_1,b_2)=\int_0^\pi\frac{d\phi}{\pi}V\big(\sqrt{b_1^2+b_2^2-2b_1b_2\cos\phi}\big), \tag{47}$$

$$\begin{aligned}&\rho_{00}=m_p^2\xi_1\xi_2,\qquad\rho_{0s}=m_p\xi_1,\\&\rho_{s0}=m_p\xi_2,\qquad\rho_{ss}=1.\end{aligned} \tag{48}$$

For low t_i the function S_2 is approximately equal to

$$\begin{aligned}F(\xi_1,\xi_2)&\equiv S_2(s/s_0,\xi_1,\xi_2,0,0)\\&\simeq\big(\sqrt{S(s/s_0,\xi_1,0)}+\sqrt{S(s/s_0,\xi_2,0)}\\&\quad-\sqrt{S(s/s_0,\xi_1,0)S(s/s_0,\xi_1,0)}\big)^2,\end{aligned} \tag{49}$$

which is clear from Figs. 12b, c. Total absorptive corrections are about 0.3–0.5 for $\xi_i<0.3$. Backgrounds can be estimated in the analogous way as in SπE.

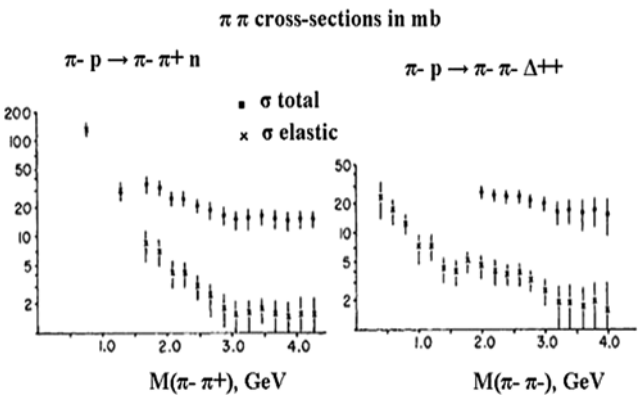

Fig. 10 Elastic and total cross-sections for $\pi^-\pi^+$ and $\pi^-\pi^-$ scattering from the data on exclusive reactions as functions of the dipion invariant mass (Fig. 5 from Ref. [5])

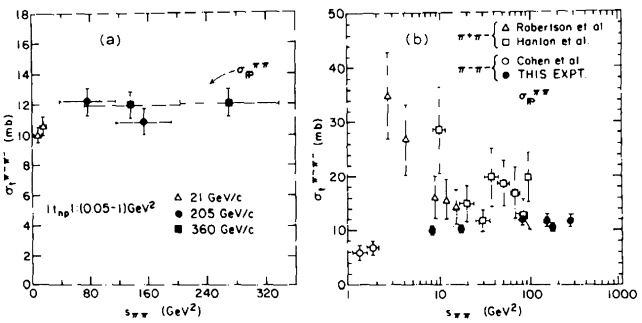

Fig. 11 Total cross-sections for $\pi^-\pi^-$ (**a**, **b**) and $\pi^+\pi^-$ (**b**) scattering from the data on inclusive $\pi^-+n\to p+X$ (**a**) and exclusive reactions as functions of the dipion invariant mass squared (Fig. 4 from Ref. [6])

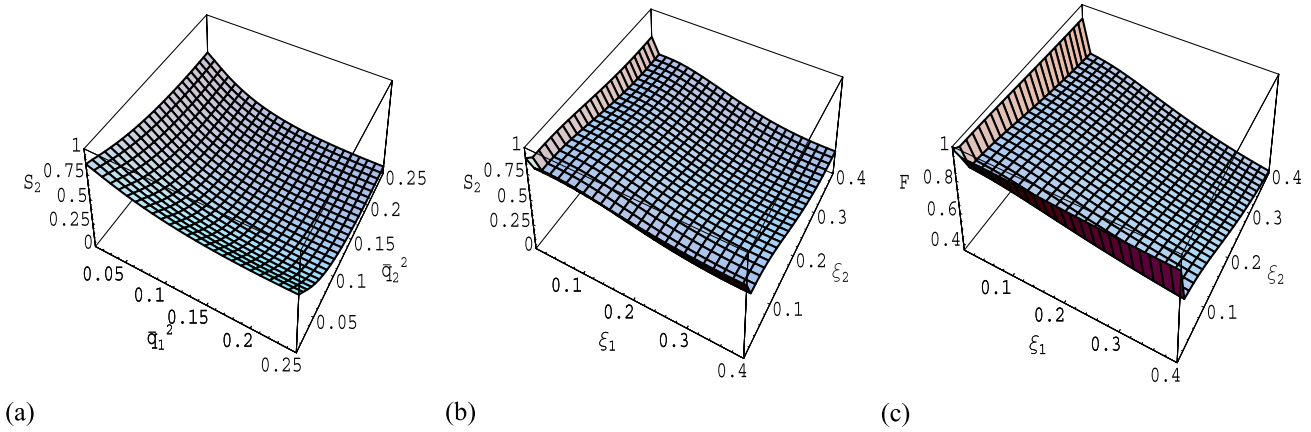

Fig. 12 The function $S_2(s/s_0, \xi_{1,2}, |\mathbf{q}_{1,2}|)$ at $\sqrt{s} = 10$ TeV: **a** for fixed $\xi_{1,2} = 0.01$, **b** for fixed $|\mathbf{q}_{1,2}| \sim 0$. **c** The function $F(\xi_1, \xi_2)$ at $\sqrt{s} = 10$ TeV

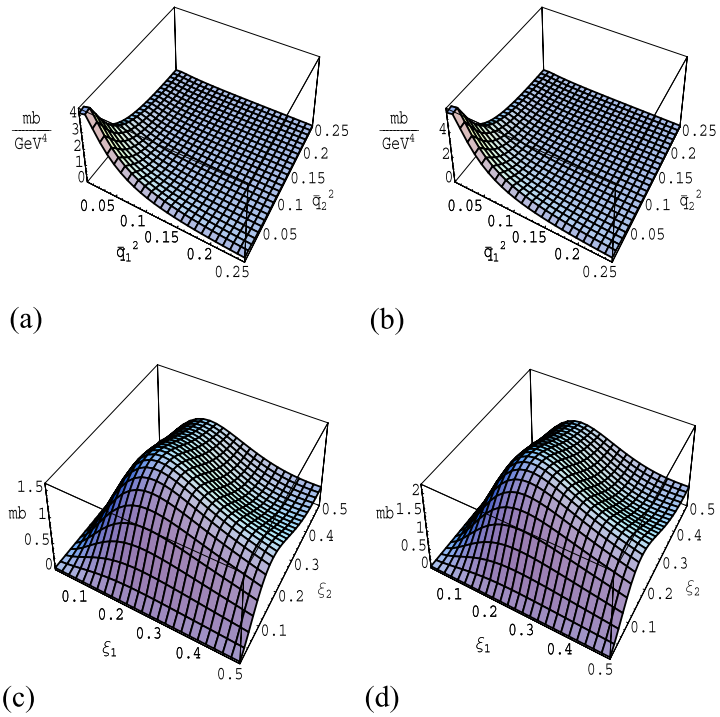

Fig. 13 Integrated double cross-sections for DπE process: $d\sigma/d\mathbf{q}_1^2\, d\mathbf{q}_2^2$, $\xi_i < 0.2$ (**a**, **b**) and $d\sigma/d\xi_1\, d\xi_2$ (**c**, **d**) for (31) (**a**, **c**) and (32) (**b**, **d**) parametrizations

To obtain $\sigma_{\pi^+\pi^+}$ we can express it from formulae (43, 44) and substitute the data on DπE differential cross-section at $\mathbf{q}_i \sim 0$. Since there are no data on this process, we can make only predictions for higher energies. Numerically calculated functions for DπE are shown in Figs. 12 and 13 and listed in Table 4 for both the Donnachie–Landshoff and COMPETE parametrizations.

Table 4 Total $p + p \to n + X + n$ cross-sections in the kinematical region $0 < |\mathbf{q}| < 0.5$ GeV, $\xi_{\min} = 10^{-6} < \xi < \xi_{\max}$ for two parametrizations (31) (32) multiplied by 2/3 (quark counting rules), i.e. $\sigma_{\pi^+\pi^+}(s) = (2/3)\sigma_{\pi^+ p}(s)$

$\xi_{\max}$	0.05	0.1	0.2	0.3
$\sigma_{p+p\to n+X+n}$, μb	0.08(0.1)	1.7(2.2)	25(33)	76(104)

5 Experimental possibilities

The single and double pion exchange process could be measured in the first few years of LHC running. As an example we will take $\sqrt{s} = 10$ TeV and focus on the CMS experiment [41]. The two Zero Degree Calorimeters (ZDC) [30, 31] could be used to measure the leading neutrons. The ZDCs are placed on the both sides of CMS 140 m away from the interaction point. They have electromagnetic

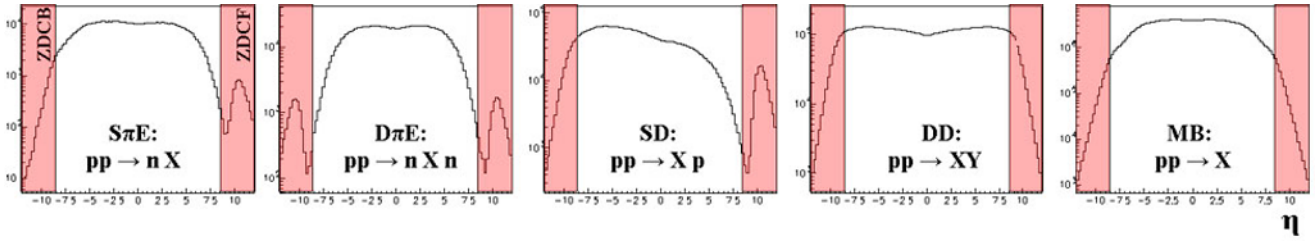

Fig. 14 Pseudorapidity distributions for signal (SπE, DπE) and background (SD, DD, MB) processes

Table 5 Ratio of SπE and background before and after selection (50)

	SπE	:	DπE	:	SD	:	DD	:	MB	S	:	B
NO (50)	1	:	0.08	:	5.4	:	3.8	:	19.2	1	:	28.4
(50)	1	:	0	:	0.8	:	0.8	:	1.2	1	:	2.7

Table 6 Ratio of DπE and background before and after selection (51)

	DπE	:	SπE	:	SD	:	DD	:	MB	S	:	B
NO (51)	1	:	13	:	70	:	49	:	250	1	:	382
(51)	1	:	0.5	:	0	:	0.8	:	0.3	1	:	1.6

and hadronic sections designed to measure photons and neutrons in the pseudorapidity region $|\eta| > 8.5$. Similar detectors have been widely used by the RHIC experiments since 2001 [42].

To study SπE and DπE processes a generator has been developed in the framework of a more general simulation package EDDE [43]. The kinematics of SπE and DπE reactions are defined by the relative energy loss of ξ_n and the square of the transverse momentum t_n for the leading neutron. The vertex $p\pi^+_{\rm virt}n$ is generated on the basis of the model described above. PYTHIA 6.420 [44] is used for the $\pi^+_{\rm virt}p \to X$ generation in the SπE and $\pi^+_{\rm virt}\pi^+_{\rm virt} \to X$ generation in the DπE. Inelastic processes, including single and double diffractive dissociation (SD and DD) and minimum bias events[1] (MB), have been studied as possible background for SπE and DπE. All background processes have been generated with PYTHIA 6.420. The cross sections for signal and background at 10 TeV have the following ratio[2]:

$$\mathrm{D}\pi\mathrm{E} : \mathrm{S}\pi\mathrm{E} : \mathrm{DD} : \mathrm{SD} : \mathrm{MB} = 0.2 : 2.6 : 9.7 : 14 : 50 \text{ mb}.$$

Figure 14 shows pseudorapidity distributions for the signal and background processes. All processes have leading neutrons in the acceptance of the ZDC, i.e. $|\eta| > 8.5$. Thus, SD, DD, and MB can imitate SπE and DπE events and SπE can be a strong background for DπE measurement.

To reduce these backgrounds we have used the following selections:

$$\begin{bmatrix} N_n^f > 0 \quad \& \quad N_n^b = 0 \quad \& \quad \xi_n^f < 0.4, \\ N_n^b > 0 \quad \& \quad N_n^f = 0 \quad \& \quad \xi_n^b < 0.4 \end{bmatrix} \tag{50}$$

for SπE and

$$\begin{cases} N_n^f > 0 \quad \& \quad N_n^b > 0, \\ \xi_n^f < 0.4 \quad \& \quad \xi_n^b < 0.4 \end{cases} \tag{51}$$

for DπE study. Here, N_n^f (N_n^b) is the number of neutrons hitting the forward (backward) ZDC, ξ_n^f (ξ_n^b) is the relative energy loss of the forward (backward) leading neutron. That is, for SπE selection we choose events with energetic neutrons in the forward or backward ZDC and with no neutrons in the opposite one. For DπE, we select events with energetic neutrons in the forward and backward ZDCs. These cuts suppress ∼90% of the background events for SπE and reduce the background for DπE by a factor of 240, see Tables 5 and 6.

Nevertheless, the signal/background ratio remains ∼1/3 for SπE and ∼2/3 for DπE. Figure 15 shows distributions of ξ and t of the leading neutron and $M = \sqrt{\xi s}$ after the cuts (50) listed above. Requiring t ($|t| < 0.25$ GeV^2) suppresses the SπE background very efficiently. Unfortunately, in the present design of ZDC this feature is supported very restrictedly.[3]

[1] Usually, MB in PYTHIA includes SπE(DπE)-like events. Here, MB means QCD non-diffractive minimum bias from PYTHIA with subtracted SπE and DπE-like processes.

[2] Cross sections for SπE and DπE are given for $\xi_n < 0.4$

[3] Electromagnetic part of ZDC could be used to measure horizontal deviation of leading neutron with 50% efficiency [45].

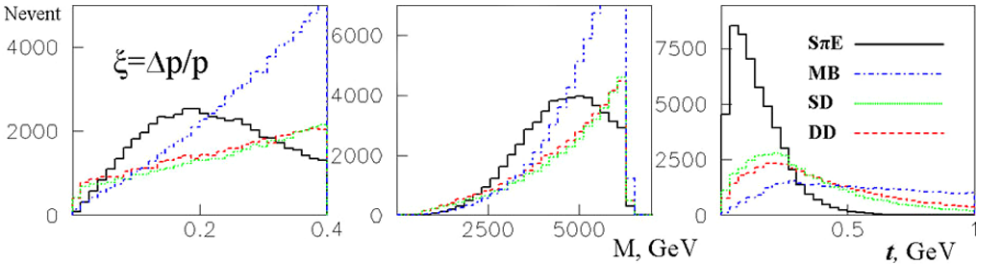

Fig. 15 Distributions of ξ and t of the leading neutron and $M = \sqrt{\xi s}$ for SπE, SD, DD and MB events (selection (50))

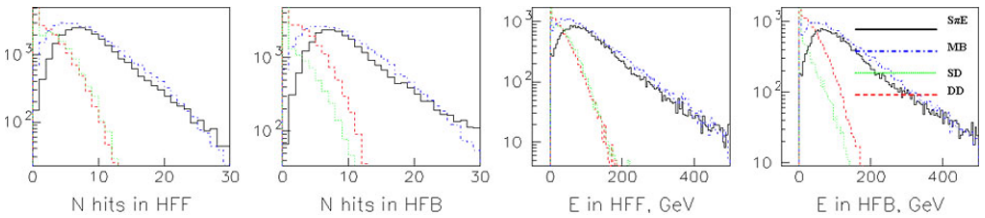

Fig. 16 Number of hits and total energy deposit in the forward and backward HF

Table 7 Ratio of SπE to background with selections (52) and (53)

	SπE	:	SD	:	DD	:	MB	S	:	B
(52)	1	:	0.013	:	0.06	:	0.48	1	:	0.56
(52)&(53)	1	:	0.005	:	0.02	:	0.055	1	:	0.08

We can of course also try to use the other CMS calorimeters to suppress the background. As an example Fig. 16 shows number of hits and the total energy deposit in the forward and backward HF for both the SπE signal and background. Requiring

$$\begin{bmatrix} N_n^f > 0 \quad \& \quad N_n^b = 0 \quad \& \quad \xi_n^f < 0.4 \quad \& \quad N_{\text{hits}}^{\text{HFB}} > 7, \\ N_n^b > 0 \quad \& \quad N_n^f = 0 \quad \& \quad \xi_n^b < 0.4 \quad \& \quad N_{\text{hits}}^{\text{HFF}} > 7 \end{bmatrix} \tag{52}$$

where $N_{\text{hits}}^{\text{HF}}$ is the number of hits in HF, makes both the SD and DD background negligible, but it has no any influence on the MB events. Table 7 shows signal/background ratios with selection (52). In the mass region below 5000 GeV we expect a signal/background ratio of ∼10/6.

To suppress the minimum bias background we cut on the t of the leading neutron:

$$|t_n| < 0.2\ \text{GeV}^2. \tag{53}$$

As shown in Table 7 this cut suppresses MB events by a factor of 8.7 and makes S/B ratio ∼100/8. Figure 17 presents M distribution for SπE and background with selections (52) and (53). The same S/B ratio for DπE process could be achieved with selections

$$N_{\text{hits}}^{\text{HFF}} > 4 \quad \& \quad N_{\text{hits}}^{\text{HFB}} > 4 \tag{54}$$

and

$$\left|t_n^f\right| < 0.3\ \text{GeV}^2 \quad \& \quad \left|t_n^b\right| < 0.3\ \text{GeV}^2. \tag{55}$$

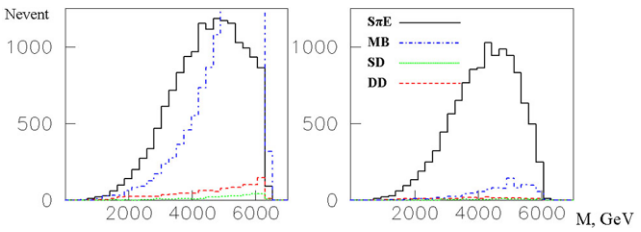

Fig. 17 $M = \sqrt{\xi_n s}$ distribution for SπE and background, selections (52) (*left*) and (53) (*right*)

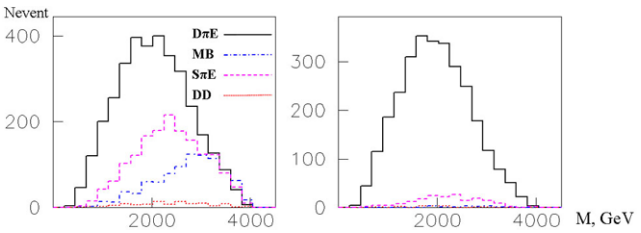

Fig. 18 Distribution in $M = \sqrt{\xi_n^f \xi_n^b s}$ for DπE and background, selections (54) (*left*) and (55) (*right*)

Table 8 shows ratios for DπE and background with selections (54) and (55). Figure 18 presents M distribution for DπE and background with selections (54) and (55).

6 Discussions and conclusions

Our generator level study shows that it could be possible to observe SπE and DπE in the first runs of CMS detector

Table 8 Ratio of DπE to background with selections (54) and (55)

	DπE	:	SπE	:	SD	:	DD	:	MB	S	:	B
(54)	1	:	0.47	:	0.0	:	0.03	:	0.2	1	:	0.7
(54)&(55)	1	:	0.06	:	0.0	:	0.005	:	0.004	1	:	0.07

at LHC. Some modifications of the ZDC is required in order to measure t of the leading neutron. Using combination of 2 simple cuts, for N hits in HF and t_n, one could suppress background by a factor of ∼760 for SπE and ∼9500 for DπE with an efficiency of ∼35% of SπE events and ∼60% of DπE. Without modifying the ZDC we expect to see SπE events mixing with MB events in the ratio SπE/MB ∼ 10/6 and DπE mixing with SπE and MB in proportions DπE/(MB + SπE) ∼ 10/(5 + 2). Thus, we could still estimate cross sections of SπE and DπE production at 10 TeV. For more realistic estimations a full MC study should be performed including detector simulation and pile-up background.

As was said the main motivation for this work is the extraction of the total πp and $\pi\pi$ cross-sections from the proton-proton scattering measurements. The procedure is quite simple at low values of t, because the absorptive factor goes to unity and backgrounds are completely suppressed. This rich data set would allow us to check predictions of different models for strong interactions, quark counting rules and so on. Our next task is an exact estimation of backgrounds presented in Figs. 1b, c, d (especially ρ, a_2 exchanges) to ensure that the extraction procedure is correct. This analysis has used several parametrizations for the total cross-sections, all of which show similar behavior. Unfortunately, the present data on SπE are not so clear (because of problems in normalization), so we can make only more or less plausible estimations for LHC energies.

The main background for the single and double pion exchange comes from minimum bias events. If we integrate over t we find a signal to background ratio for SπE and DπE is about 1.5–2. It can be increased significantly only if we use a cut $|t| < 0.2$–0.3 GeV^2 (which was done, for example, in low-energy experiments). Since a precision measurement of t_n is not possible with the present design of the ZDC, precise extraction of πp and $\pi\pi$ cross-sections will have to await an upgrade of the ZDC [45]. Nevertheless, we should be able to get rough estimates of the πp and $\pi\pi$ cross-sections in the first LHC run.

It should be noted that the ALICE and ATLAS, ZDCs have more advanced designs than the CMS ZDC. The ATLAS ZDC [46] has a complex structure consisting of quartz rods and strips, that allows to measure coordinates of neutron hits with spatial resolution better than 1 mm for high energy neutrons. This corresponds to t-resolution $\delta t/|t| \sim 0.2/\sqrt{|t|[\mathrm{GeV}^2]}$ for 5 TeV neutrons at 140 m, which should allow for an effective background suppression as well as for

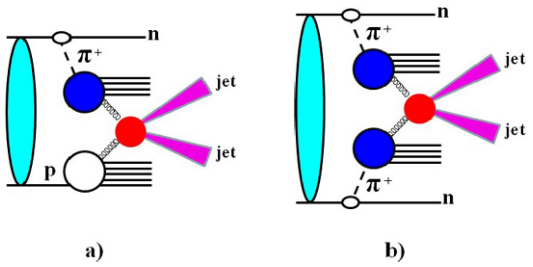

Fig. 19 Processes for the measurements of parton distributions in pions

the extraction of $\pi^+ p$ and $\pi^+\pi^+$ total cross section. The ALICE ZDC [47] is segmented into 4 independent towers in the front cross section, which is not sufficient for a precise measurement of t but should still allow some measurement of single and double pion exchange [48].

By looking at leading neutrons in combination with two jets it may be possible to study the parton distribution of the pion at low x and high Q^2. This process is shown in Fig. 19. However cross-sections for hard processes are small so this measurement will have to wait for high luminocity runs. It seems to be fairly realistic, especially taking into account new prospects for high-energy πp interactions. The investigation of SπE and DπE processes can also provide us with unique measurements of πp and $\pi\pi$ elastic cross-sections.

In conclusion we reiterate that measuring the πp and $\pi\pi$ total cross-sections at several TeV is of exceptional importance. The physics potential of these cross sections will easily justify the effort required for their measurement.

Acknowledgements We are grateful to M. Albrow, M. Arneodo, V.I. Kryshkin, M. Murray, K. Piotrzkowski and N.E. Tyurin for useful discussions and helpfull suggestions. V.A.P. thanks M.G. Ryskin for stimulating comments on inclusive neutron production. We also thanks M. Murray and J.-P. Guillaud for corrections.

References

1. G.F. Chew, F.E. Low, Phys. Rev. **113**, 1640 (1959)
2. C. Goebel, Phys. Rev. Lett. **1**, 337 (1958)
3. J.T. Carroll, J.A.J. Matthews, W.D. Walker, M.W. Firebaugh, J.D. Prentice, T.S. Yoon, Phys. Rev. D **10**, 1430 (1974)
4. B.Y. Oh, A.F. Garfinkel, R. Morse, W.D. Walker, J.D. Prentice, E.C. West, T.S. Yoon, Phys. Rev. D **1**, 2494 (1970)
5. W.J. Robertson, W.D. Walker, J.L. Davis, Phys. Rev. D **7**, 2554 (1973)
6. H. Abramowicz et al., Nucl. Phys. B **166**, 62 (1980)

7. J. Breitweg et al. (ZEUS Collaboration) Eur. Phys. J. C **2**, 247 (1998)
8. M.G. Ryskin, Y.M. Shabelski, Phys. At. Nucl. **61**, 81 (1998) Yad. Fiz. **61**, (1998) 89
9. P. Soding, Phys. Lett. **19**, 702 (1966)
10. M. Derrick et al. (ZEUS Collaboration), Phys. Lett. B **384**, 388 (1996)
11. J. Breitweg et al., Nucl. Phys. B **596**, 3 (2001)
12. J. Breitweg et al., Eur. Phys. J. C **1**, 81 (1998)
13. J. Breitweg et al., Eur. Phys. J. C **2**, 237 (1998)
14. S. Chekanov et al. (ZEUS Collaboration), Nucl. Phys. B **637**, 3 (2002)
15. S. Chekanov et al. (ZEUS Collaboration), Phys. Lett. B **610**, 199 (2005)
16. C. Adloff et al. (H1 Collaboration), Eur. Phys. J. C **6**, 587 (1999)
17. C. Adloff et al. (H1 Collaboration), Nucl. Phys. B **619**, 3 (2001)
18. W. Flauger, F. Monnig, Nucl. Phys. B **109**, 347 (1976)
19. J. Engler et al., Nucl. Phys. B **84**, 70 (1975)
20. S.J. Barish et al., Phys. Rev. D **12**, 1260 (1975)
21. B. Robinson et al., Phys. Rev. Lett. **34**, 1475 (1975)
22. Y. Eisenberg et al., Nucl. Phys. B **135**, 189 (1978)
23. D. Vagra (NA49 Collaboration), Eur. Phys. J. C **33**, S515 (2004)
24. M. Togawa (for the PHENIX Collaboration), Measurement of the cross section and the single transverse spin asymmetry in very forward neutron production from polarized pp collisions at RHIC, in *Forward Physics and QCD*, Hamburg, 2007, pp. 308–315
25. A.B. Kaidalov, V.A. Khoze, A.D. Martin, M.G. Ryskin, Eur. Phys. J. C **47**, 385 (2006)
26. V.A. Khoze, A.D. Martin, M.G. Ryskin, Eur. Phys. J. C **48**, 797 (2006)
27. B.Z. Kopeliovich, I.K. Potashnikova, I. Schmidt, J. Soffer, Phys. Rev. D **78**, 014031 (2008)
28. B.Z. Kopeliovich, I.K. Potashnikova, I. Schmidt, J. Soffer, AIP Conf. Proc. **1056**, 199 (2008)
29. V.A. Petrov, A.V. Prokudin, Eur. Phys. J. C **23**, 135 (2002)
30. A.S. Ayan et al., CMS-IN-2006/54
31. O.A. Grachov et al. (CMS Collaboration), J. Phys. Conf. Ser. **160**, 012059 (2009)
32. V. Stoks, R. Timmermans, J.J. de Swart, Phys. Rev. C **47**, 512 (1993)
33. R.A. Arndt, I.I. Strakovsky, R.L. Workman, M.M. Pavan, Phys. Rev. C **52**, 2120 (1995)
34. B.Z. Kopeliovich, B. Povh, I. Potashnikova, Z. Phys. C **73**, 125 (1996)
35. K.G. Boreskov, A.B. Kaidalov, L.A. Ponomarev, Sov. J. Nucl. Phys. **19**, 565 (1974)
36. K.G. Boreskov, A.B. Kaidalov, V.I. Lisin, E.S. Nikolaevskii, L.A. Ponomarev, Sov. J. Nucl. Phys. **15**, 203 (1972)
37. E. Ferrari, Nucl. Phys. B **98**, 109 (1975)
38. A. Donnachie, P.V. Landshoff, Phys. Lett. B **296**, 227 (1992)
39. B. Nicolescu et al. (COMPETE Collaboration), in *Elastic and Diffractive Scattering*, Pruhonice, 2001, pp. 265–274. arXiv:hep-ph/0110170
40. Particle Data Group $\pi^+ p$ real cross-sections data
41. The compact muon solenoid. Technical Proposal, CERN/LHCC-94-38, LHCC/P1
42. A. Clemens, A. Denisov, E. Garcia, M. Murray, H. Strobele, S. White, Nucl. Instrum. Methods A **470**, 488 (2001)
43. V.A. Petrov, R.A. Ryutin, A.E. Sobol, J.-P. Guillaud, arXiv:0711.1794 [hep-ph]
44. T. Sjostrand, S. Mrenna, P. Skands, J. High Energy Phys. **0605**, 026 (2006)
45. M. Murray, private communications
46. ATLAS Collaboration, CERN/LHCC/2007-001
47. M. Gallio et al., ALICE-DOC-2004-003
48. J.G. Contreras, ALICE-INT-2006-007